Finite-Element Time-Domain Algorithms for Modeling Linear Debye and Lorentz Dielectric Dispersions at Low Frequencies

Nikolay S. Stoykov*, *Member, IEEE*, Todd A. Kuiken, *Member, IEEE*, Madeleine M. Lowery, *Member, IEEE*, and Allen Taflove, *Fellow, IEEE*

***Abstract*—We present what we believe to be the first algorithms that use a simple scalar-potential formulation to model linear Debye and Lorentz dielectric dispersions at low frequencies in the context of finite-element time-domain (FETD) numerical solutions of electric potential. The new algorithms, which permit treatment of multiple-pole dielectric relaxations, are based on the auxiliary differential equation method and are unconditionally stable. We validate the algorithms by comparison with the results of a previously reported method based on the Fourier transform. The new algorithms should be useful in calculating the transient response of biological materials subject to impulsive excitation. Potential applications include FETD modeling of electromyography, functional electrical stimulation, defibrillation, and effects of lightning and impulsive electric shock.**

***Index Terms*—Finite element methods, transient analysis.**

I. Introduction

THE electrical properties of dielectric materials inevitably vary with frequency. This phenomenon is termed dielectric dispersion. In the time domain, dispersion leads to a convolutional relation between an impulsive excitation and the effective dielectric impulse response. The dielectric dispersion properties of biological tissues have been studied extensively. A number of theoretical and empirical models are available to explain the large volume of measured data [1]–[7]. However, few if any published computational simulations of tissue interactions with low-frequency electric fields account for any dielectric dispersion. This holds for a variety of electrical signals within the body, for example those due to muscle action potentials, heart and brain activity, and functional electrical stimulation. Until recently, it has been thought that tissue dielectric dispersion has little effect on such electrical responses [8]. In fact, it has even been generally assumed that tissue displacement currents are unimportant [9]. Recently, we explored the importance of tissue displacement currents and dielectric dispersion at low frequencies [8]. We employed a commercial finite-element time-domain (FETD) code [10] to model the propagation of an action potential along a single muscle fiber in a homogeneous tissue medium. The results of our study indicate that valuable physical information can be lost if displacement currents and dispersion are disregarded. While the FETD code used in [8] can treat displacement currents, it cannot deal with frequency-dependent dielectric permittivity. As a result, we were constrained to model only homogeneous media, and were compelled to use a complicated procedure involving Fourier transformation to obtain broad spectral data. These are serious deficiencies if one desires to model realistic anatomical structures subject to realistic electrical waveforms. Subsequently, we were motivated to explore the availability of computational methods capable of straightforward modeling of electrical signals propagating within inhomogeneous, frequency dispersive biological tissues. For frequencies above about 1 MHz, the finite-difference time-domain (FDTD) method [11] is a popular approach for such modeling. FDTD can readily incorporate dielectric dispersions having an arbitrary number of Debye and Lorentz poles. However, FDTD has not yet been extended fully to the low-frequency range that is of interest here for biological tissue structures having arbitrary inhomogeneities and subject to arbitrary excitations. At frequencies well below 1 MHz (appropriate for studies of the body's own electrical signaling network and many diagnostic and therapeutic procedures), we believe that the FETD technique is currently the only available computational approach that permits the required level of realistic modeling of general time-dependent phenomena and arbitrary structures. The full-wave approach of [12] permits FETD modeling of both Debye and Lorentz dielectric dispersions with multiple poles. However, this formulation yields an unnecessarily high computational burden for low-frequency bioelectric field problems where a scalar-potential approach is sufficient. With this motivation, we report in this paper two new FETD algorithms for efficient modeling of dispersive dielectric properties at low frequencies where eddy currents and wave phenomena are unimportant [9], [13]. Based upon a scalar-potential formulation and the auxiliary differential equation (ADE) technique (originally applied to model dispersion in the context of FDTD [11]), the new algorithms can treat multiple-pole Debye and Lorentz dispersions much more simply than the approach in [12]. Further,

Manuscript received November 1, 2002; revised January 30, 2003. This work was supported in part by a grant from the Institute for Bioengineering and Nanoscience in Advanced Medicine (IBNAM) of Northwestern University, and by the National Institute of Disability and Rehabilitation Research under Grant H133G990074-00. *Asterisk indicates corresponding author.*

*N. S. Stoykov is with the Rehabilitation Institute of Chicago, IL 60611 USA, and with the Department of Physical Medicine and Rehabilitation, Northwestern University, Chicago, IL 60611 USA (e-mail: n-stoykov@northwestern.edu).

T. A. Kuiken and M. M. Lowery are with the Rehabilitation Institute of Chicago, IL 60611 USA and also with the Department of Physical Medicine and Rehabilitation and the Department of Electrical and Computer Engineering, Northwestern University, Chicago, IL 60611 USA.

A. Taflove is with the Department of Electrical and Computer Engineering, Northwestern University, Evanston, IL 60208 USA.

Digital Object Identifier 10.1109/TBME.2003.816083

the algorithms retain all of the capabilities of previous nondispersive finite-element methods with respect to flexibility in simulating spatially inhomogeneous structures of arbitrary shape. Section II of this paper presents the theoretical basis of the dispersive formulation. Section III presents the FETD algorithms for the cases of multiple-pole Debye and Lorentz dispersions. Section IV discusses the numerical implementation. Section V reports validation studies, which illustrate the accuracy of the new techniques. Finally, Section VI concludes the paper with a discussion of future work.

II. Theoretical Basis of Dispersive Formulation

The Debye dispersion is characterized by the following expression for the relative permittivity, ε_r, as a function of the angular frequency, ω [11]:

$$\varepsilon_r(\omega) = \varepsilon_\infty + \sum_{p=1}^{P} \frac{\Delta\varepsilon_p}{1+j\omega\tau_p} \equiv \varepsilon_r'(\omega) - j\varepsilon_r''(\omega) \qquad (1)$$

where τ_p is the relaxation time of the pth Debye pole, $\Delta\varepsilon_p$ is the corresponding relative permittivity increment, and ε_r', ε_r'' are the real and the complex part of the relative permittivity. From (1) it is clear that $\varepsilon_r(0) = \varepsilon_\infty + \Delta\varepsilon_1 + \cdots + \Delta\varepsilon_P$, and $\lim_{\omega\to+\infty} \varepsilon_r(\omega) = \varepsilon_\infty$. Further, while ε_r rapidly decreases in the vicinity of each pole frequency, $1/\tau_p$, there is little change elsewhere. The defining expression for the Lorentz dispersion is [11]

$$\varepsilon_r(\omega) = \varepsilon_\infty + \sum_{p=1}^{P} \frac{\Delta\varepsilon_p\omega_p^2}{\omega_p^2 + 2j\omega\delta_p - \omega^2} \equiv \varepsilon_r'(\omega) - j\varepsilon_r''(\omega) \quad (2)$$

where ω_p is the undamped resonant frequency of the pth Lorentz pole-pair, δ_p is the corresponding damping factor, and $\Delta\varepsilon_p$ is the corresponding relative permittivity increment. Again, $\varepsilon_r(0) = \varepsilon_\infty + \Delta\varepsilon_1 + \cdots + \Delta\varepsilon_P$, and ε_∞ is the high-frequency limit of the relative permittivity. The terms in (2) can be regarded as pole-pairs because each denominator has two complex roots. The resonant nature of the Lorentz dispersion can be easily recognized in (2): the contribution of the pth pole-pair to the total relative permittivity increases as ω approaches ω_p but remains finite if δ_p is greater than zero.

As discussed in [11], multipole dispersion can be accounted for by adding polarization current terms to the right-hand side of the Maxwell-Ampere Law

$$\nabla\times\vec{H}(t) = \sigma\vec{E}(t) + \varepsilon_0\varepsilon_\infty\frac{\partial}{\partial t}\vec{E}(t) + \sum_{p=1}^{P}\vec{J}_p(t). \qquad (3)$$

Here, $\vec{H}$ and $\vec{E}$ denote the magnetic and electric field intensities, ε_0 is the permittivity of vacuum, and ε_∞ is the high-frequency limit of the relative permittivity as defined in (1) and (2). $\vec{J}_p$ is the contribution of the pth Debye pole or pth Lorentz pole-pair to the total polarization current. We need to specify this contribution before proceeding with the derivation of the computational algorithms.

There are two standard numerical methods to obtain $\vec{J}_p(t)$ for Debye and Lorentz dispersions, the piecewise linear recursive convolution (PLRC) method, and the ADE method [11]. Both techniques have been successfully employed to derive FDTD algorithms for high-frequency problems involving electromagnetic wave interactions. For the low-frequency problem at hand, we choose the ADE method because it can be integrated into the general FETD scheme quite naturally.

Following the general ADE approach, we first express $\vec{J}_p$ in the frequency domain as a function of $\vec{E}$ and the frequency-dependent material properties. For example, we have

$$\vec{J}_p(\omega) = \varepsilon_0\Delta\varepsilon_p\left(\frac{j\omega}{1+j\omega\tau_p}\right)\vec{E}(\omega) \qquad (4)$$

for Debye materials and

$$\vec{J}_p(\omega) = \varepsilon_0\Delta\varepsilon_p\omega_p^2\left(\frac{j\omega}{\omega_p^2 + 2j\omega\delta_p - \omega^2}\right)\vec{E}(\omega) \qquad (5)$$

for Lorentz materials. We multiply both sides of (4) by $(1 + j\omega\tau_p)$ and both sides of (5) by $(\omega_p^2 + 2j\omega\delta_p - \omega^2)$, and then use the inverse Fourier transformation to obtain

$$\vec{J}_p(t) + \tau_p\frac{d}{dt}\vec{J}_p(t) = \varepsilon_0\Delta\varepsilon_p\frac{d}{dt}\vec{E}(t) \qquad (6)$$

and

$$\omega_p^2\vec{J}_p(t) + 2\delta_p\frac{d}{dt}\vec{J}_p(t) + \frac{d^2}{dt^2}\vec{J}_p(t) = \varepsilon_0\Delta\varepsilon_p\omega_p^2\frac{d}{dt}\vec{E}(t) \quad (7)$$

respectively. Equations (6) and (7) are the desired ADEs for Debye and Lorentz materials. The initial conditions are $\vec{J}_p(0) = 0$ for (6) and $\vec{J}_p(0) = 0$, $d\vec{J}_p/dt|_{t=0} = 0$ for (7).

III. Solution Approach

The next step is to solve (3) and (6) for Debye materials, and (3) and (7) for Lorentz materials in the context of the FETD technique. In each case, the starting point is a system of differential equations rather than a variational principle, so we will use Galerkin's method to discretize this system and derive the corresponding set of linear algebraic equations. Since the differential equations are formulated in the time domain, they will first be discretized in space and then in time, a widely used two-step approach [14].

A. Derivation of the Weighted-Residuals Version of the Low-Frequency Maxwell-Ampere Law

We first take the divergence of both sides of (3) to eliminate $\vec{H}$, since the divergence of the curl of a function vanishes identically. Then, we multiply both sides by the piecewise continuously differentiable scalar function $\psi(x,y,z)$ and integrate over the solution domain, Ω. This yields

$$\int_\Omega \psi\nabla\cdot\left[\sigma\vec{E}(t) + \varepsilon_0\varepsilon_\infty\frac{\partial}{\partial t}\vec{E}(t) + \sum_{p=1}^{P}\vec{J}_p(t)\right]d\Omega = 0. \quad (8)$$

Integrating by parts, we obtain

$$\begin{aligned}\int_{\partial\Omega}\psi\sigma E_n dS - \int_\Omega \sigma\vec{E}\cdot\nabla\psi d\Omega \\ + \int_{\partial\Omega}\psi\varepsilon_0\varepsilon_\infty\frac{\partial E_n}{\partial t}dS - \int_\Omega\varepsilon_0\varepsilon_\infty\frac{\partial\vec{E}}{\partial t}\cdot\nabla\psi d\Omega \\ + \sum_{p=1}^{P}\int_{\partial\Omega}\psi J_{p,n} - \sum_{p=1}^{P}\int_\Omega\vec{J}_p\nabla\psi d\Omega = 0 \end{aligned} \qquad (9)$$

where $\partial\Omega$ denotes the boundary of the solution domain, and the subscript n indicates the outward normal component of the cor-

responding vector. The surface integrals in (9) can be expressed by a single integral

$$\int_{\partial\Omega} \psi \left(\sigma E_n + \varepsilon_0 \varepsilon_\infty \frac{\partial E_n}{\partial t} + \sum_{p=1}^{P} J_{p,n} \right) dS. \tag{10}$$

The three terms grouped within the parentheses in (10) are, respectively, the normal component of the conduction current density, the displacement/polarization current density at infinite frequency, and the polarization current density due to the dispersive nature of the medium. These terms are included in the total normal current density, $-J_n$, at $\partial\Omega$. It is $-J_n$ that is specified whenever the current is a part of the boundary conditions. The negative sign is used to comply with the convention used here that inward flowing currents at $\partial\Omega$ are considered positive.

To bring (9) into a more symmetric form, we use the fact that, in low-frequency problems, $\vec{E}$ is a gradient field. Such fields can be expressed solely in terms of the electric scalar potential, φ

$$\vec{E}(t) = -\nabla\varphi(t). \tag{11}$$

Using (11), we can rewrite (9) as

$$\int_{\Omega} \sigma \nabla\varphi \nabla\psi d\Omega + \int_{\Omega} \varepsilon_0 \varepsilon_\infty \nabla \frac{\partial \varphi}{\partial t} \nabla\psi d\Omega + \sum_{p=1}^{P} \int_{\Omega} \vec{J}_p \nabla\psi d\Omega = \int_{\partial\Omega} \psi J_n dS. \tag{12}$$

Equation (12) is the weighted-residuals version of the low-frequency Maxwell-Ampere Law (LFMAL). The integral in the third term on the left-hand side of (12) can be written in the same form as those in the first two terms, because (6) and (7) and their homogeneous initial conditions imply that $\vec{J}_p$ and the time-derivative of $\vec{E}$ are always collinear. Hence, $\vec{J}_p$ can be written in the form

$$\vec{J}_p = \vartheta_p \nabla \frac{\partial \varphi(t)}{\partial t} \tag{13}$$

where ϑ_p is a space- and time-dependent scalar multiplicative factor.

B. Discretization in Space of the Weighted-Residuals Version of LFMAL

Equation (12) can now be discretized in space according to a standard procedure for the Helmholtz equation [15]. Using the interpolation functions as weighting functions as per Galerkin's method, for each element k we first calculate the matrix

$$S_k = \int_{\Omega_k} \nabla\psi_i \nabla\psi_j d\Omega \tag{14}$$

where Ω_k is the space occupied by the element, and ψ_i and ψ_j are the interpolating functions centered at nodes i and j. If nodes i and j are connected with element k, then the corresponding matrix term, $S_k(i,j)$, can be easily calculated [15]. If nodes i and j are not connected with element k, then $S_k(i,j)$ is zero. Equation (12) yields at the kth element

$$\sigma_k S_k \Phi + \varepsilon_0 \varepsilon_{\infty,k} S_k \frac{\partial \Phi}{\partial t} + \sum_{p=1}^{P} \vartheta_{p,k} S_k \frac{\partial \Phi}{\partial t} = I_k \tag{15}$$

where σ_k and $\varepsilon_{\infty,k}$ are the (constant) values of the material properties within the kth element; $\vartheta_{p,k}$ is the unknown multiplicative factor from (13) that is constant within the kth element; and Φ is the unknown global vector of the nodal potential. I_k depends on any prescribed nonzero voltage in Ω or at $\partial\Omega$, but for the sake of simplicity we assume that only zero voltage (ground) can be prescribed. Therefore, I_k is the total normal current for the kth element, if this element has one or more faces located along $\partial\Omega$. I_k is zero otherwise. To further simplify our notation we introduce the quantity $G_{p,k}$, which is associated with the kth element

$$G_{p,k} = \vartheta_{p,k} S_k \frac{\partial \Phi}{\partial t}. \tag{16}$$

C. Discretization in Time of the Weighted-Residuals Version of LFMAL

The second step, discretization in time, can be performed independently of the first step. In particular, the order of the approximation in time may be different from the order of approximation in space. For example, the approximation in space may be linear, while the approximation in time may be quadratic. This fact is important in the case of Lorentz materials, since the corresponding auxiliary differential equation (7) is of second order and cannot be discretized with linear elements in time. In the case of Debye materials, linear elements can be used in time and (15) can be cast into the following form if Galerkin's method is applied [15]:

$$(3\varepsilon_0\varepsilon_{\infty,k} + 2\sigma_k\Delta t) S_k \Phi^{n+1} - (3\varepsilon_0\varepsilon_{\infty,k} - \sigma_k\Delta t) S_k \Phi^n + \left(2\sum_{p=1}^{P} G_{p,k}^{n+1} + \sum_{p=1}^{P} G_{p,k}^{n} \right) \Delta t = 2I_k^{n+1} + I_k^n. \tag{17}$$

The superscripts in (17) refer to the time at which the corresponding variable is evaluated measured in time-steps, and Δt is the length of the time-step. We note that the linear approximation implemented with finite elements in time yields the same result as the linear approximation in time implemented with the PLRC method [11]. If quadratic approximation in time is used, (15) transforms into [14]:

$$\begin{aligned}(\gamma\varepsilon_0\varepsilon_{\infty,k} + \beta\Delta t\sigma_k) S_k \Phi^{n+1} &+ \left[(1-2\gamma)\varepsilon_0\varepsilon_{\infty,k} + \left(\frac{1}{2} - 2\beta + \gamma \right) \Delta t \sigma_k \right] S_k \Phi^n \\ &+ \left[(\gamma-1)\varepsilon_0\varepsilon_{\infty,k} + \left(\frac{1}{2} + \beta - \gamma \right) \Delta t \sigma_k \right] S_k \Phi^{n-1} + f = h\Delta t^2\end{aligned} \tag{18}$$

where

$$f = \beta \sum_{p=1}^{P} G_p^{n+1} + \left(\frac{1}{2} - 2\beta + \gamma \right) \sum_{p=1}^{P} G_p^n + \left(\frac{1}{2} + \beta - \gamma \right) \sum_{p=1}^{P} G_p^{n-1} \tag{19}$$

and

$$h = \beta I^{n+1} + \left(\frac{1}{2} - 2\beta + \gamma \right) I^n + \left(\frac{1}{2} + \beta - \gamma \right) I^{n-1} \tag{20}$$

and the parameters β and γ assume different values for different weighting functions in time. For example, the choice of $\beta = 4/5$

and $\gamma = 3/2$ corresponds to the weighting functions used by Galerkin's method. For the "average acceleration" weighting functions, these values are $\beta = 1/4$ and $\gamma = 1/2$. Note that the choice of β and γ can influence the numerical stability of the time-stepping scheme, which will be addressed later.

D. Discretization of the ADE

We next provide updating procedures for G_p^n. Such procedures can be inferred from the ADEs.

1) Debye Materials: In the case of Debye materials, we use Galerkin's method with linear approximation in time [15] and obtain the following result from (6):

$$\begin{aligned}\vec{J}_p^{n+1} &= \frac{3\tau_p - \Delta t}{3\tau_p + 2\Delta t}\vec{J}_p^n + \frac{3\varepsilon_0\Delta\varepsilon_p}{3\tau_p + 2\Delta t}(\vec{E}^{n+1} - \vec{E}^n) \\ &\equiv a_p\vec{J}_p^n + b_p(\vec{E}^{n+1} - \vec{E}^n). \end{aligned} \tag{21}$$

We next apply the same technique to discretize (21) in space as with (3). That is, we take the divergence of both sides of (21), multiply by ψ and integrate over Ω. This yields

$$\begin{aligned}\int_\Omega \psi\nabla\cdot\vec{J}_p^{n+1}d\Omega &= \int_\Omega \psi\nabla\cdot\left(a_p\vec{J}_p^n\right)d\Omega \\ &\quad + \int_\Omega \psi\nabla\cdot\left[b_p(\vec{E}^{n+1} - \vec{E}^n)\right]d\Omega \end{aligned} \tag{22}$$

Integration by parts yields

$$\begin{aligned}\int_{\partial\Omega} \psi J_{p,n}^{n+1}dS - \int_\Omega \vec{J}_p^{n+1}\nabla\psi d\Omega &= \int_{\partial\Omega}\psi a_p J_{p,n}^n dS - \int_\Omega a_p\vec{J}_p^n\nabla\psi d\Omega \\ &\quad + \int_{\partial\Omega}\psi\left(b_pE_n^{n+1} - b_pE_n^n\right)dS \\ &\quad - \int_\Omega b_p(\vec{E}^{n+1} - \vec{E}^n)\nabla\psi d\Omega. \end{aligned} \tag{23}$$

Again, the subscript n in the surface integrals of (23) denotes the outward normal component of the corresponding vector with respect to the surface.

Equation (23) represents a relation between the volume integrals only, because the surface integrals cancel each other out. To see this, we note that (21) implies

$$J_{p,n}^{n+1} = a_pJ_{p,n}^n + b_p\left(E_n^{n+1} - E_n^{n+1}\right). \tag{24}$$

Multiplying both sides of (24) by ψ and integrating over $\partial\Omega$ proves the cancellation.

With (11), (23) simplifies to

$$\int_\Omega \vec{J}_p^{n+1}\nabla\psi d\Omega = \int_\Omega a_p\vec{J}_p^n\nabla\psi d\Omega + \int_\Omega b_p\nabla(\varphi^{n+1} - \varphi^n)\nabla\psi d\Omega. \tag{25}$$

This can be immediately discretized in space by using standard procedures [15]. For element number k, we obtain

$$G_{p,k}^{n+1} = a_{p,k}G_{p,k}^n + b_{p,k}S_k(\Phi^{n+1} - \Phi^n). \tag{26}$$

Here, the values of a and b vary in space but are considered to be the constants, a_k and b_k, within each element; S_k is the Dirichlet matrix of the kth element normalized with respect to the material properties [15]. Φ^0 and $G_{p,k}^0$ are available from the initial conditions.

2) Lorentz Materials: In the case of Lorentz materials, we use the general method of weighted residuals and quadratic approximation in time as described in [14]. Equation (7) then yields

$$\begin{aligned}&\left(1+2\Delta_p\gamma\Delta t+\omega_p^2\beta\Delta t^2\right)\vec{J}_p^{n+1} \\ &\quad = \left[2-2\Delta_p(1-2\gamma)\Delta t-\omega_p^2\left(\frac{1}{2}-2\beta+\gamma\right)\Delta t^2\right]\vec{J}_p^n \\ &\quad\quad -\left[1-2\Delta_p(1-\gamma)\Delta t+\omega_p^2\left(\frac{1}{2}+\beta-\gamma\right)\Delta t^2\right]\vec{J}_p^{n-1} \\ &\quad\quad +g_p\left[\gamma\vec{E}^{n+1}+(1-2\gamma)\vec{E}^n-(1-\gamma)\vec{E}^{n-1}\right] \end{aligned} \tag{27}$$

where

$$g_p = \varepsilon_0\Delta\varepsilon_p\omega_p^2\Delta t. \tag{28}$$

We discretize (27) in the same way as we did in the case of Debye materials and obtain

$$\begin{aligned}A_{p,k}G_{p,k}^{n+1} &= B_{p,k}G_{p,k}^n - C_{p,k}G_{p,k}^{n-1} \\ &\quad + g_{p,k}S_k\left[\gamma\Phi^{n+1} + (1-2\gamma)\Phi^n - (1-\gamma)\Phi^{n-1}\right]. \end{aligned} \tag{29}$$

Equation (29) refers to the kth element, where $A_{p,k}$, $B_{p,k}$, $C_{p,k}$ are the values of the coefficients in front of $\vec{J}_p^{n+1}$, $\vec{J}_p^n$ and $\vec{J}_p^{n-1}$ in (27), and $g_{p,k}$ is the value of g_p from (28).

E. Completion of the Algorithms

1) Debye Materials: Equation (26) allows us to eliminate $G_{p,k}^{n+1}$ from (17), which becomes

$$\begin{aligned}&\left(3\varepsilon_0\varepsilon_{\infty,k}+2\sigma_k\Delta t+\sum_{p=1}^P\frac{6\varepsilon_0\Delta\varepsilon_p\Delta t}{3\tau_p+2\Delta t}\right)S_k\Phi^{n+1} \\ &\quad -\left(3\varepsilon_0\varepsilon_{\infty,k}-\sigma_k\Delta t+\sum_{p=1}^P\frac{6\varepsilon_0\Delta\varepsilon_p\Delta t}{3\tau_p+2\Delta t}\right)S_k\Phi^n \\ &\quad +\sum_{p=1}^P\left(1+\frac{6\tau_p-2\Delta t}{3\tau_p+2\Delta t}\right)\Delta tG_p^n = 2I_k^{n+1}+I_k^n. \end{aligned} \tag{30}$$

The only unknown variable in (30) for $n = 0$ is Φ^1. It can be calculated if the left-hand and right-hand sides of (30) are obtained and summed over all elements. This is the well-known process of assembling the global matrices. If Φ^n is available for $n = m$ and $n = m + 1$, and $G_{p,k}^n$ is available for $n = m$, then $G_{p,k}^{n+1}$ can be obtained from (26). Now we can obtain Φ^{n+2} by substituting Φ^{n+1} and $G_{p,k}^{n+1}$ in (30), which completes the algorithm.

2) Lorentz Materials: Equation (29) allows us to eliminate $G_{p,k}^{n+1}$ from (18), which for $A_{p,k} \neq 0$ becomes

$$\begin{aligned}&\left(\gamma\varepsilon_0\varepsilon_{\infty,k}+\beta\Delta t\sigma_k+\beta\gamma\sum_{p=1}^P\frac{g_{p,k}}{A_{p,k}}\right)S_k\Phi^{n+1} \\ &\quad +\left[(1-2\gamma)\varepsilon_0\varepsilon_{\infty,k}+\left(\frac{1}{2}-2\beta+\gamma\right)\Delta t\sigma_k\right.\end{aligned}$$

TABLE I
PARAMETERS OF THE SIMULATED DISPERSIVE MATERIALS

	σ_{dc} (S/m)	ε_∞	$\Delta\varepsilon$	τ_p (s)	δ_p (rad/s)	ω_p (rad/s)
Debye	7.620×10^{-2}	4.300×10^{0}	8.000×10^{5}	2.306×10^{-3}	N/A	N/A
			8.190×10^{4}	3.701×10^{-6}	N/A	N/A
			1.190×10^{4}	2.375×10^{-7}	N/A	N/A
			3.200×10^{1}	6.920×10^{-10}	N/A	N/A
			4.580×10^{1}	7.958×10^{-12}	N/A	N/A
Lorentz	2.000×10^{-3}	1.000×10^{-3}	1.000×10^{9}	N/A	1.000×10^{0}	$2\pi \times 10^{1}$
			1.000×10^{9}	N/A	1.000×10^{1}	$2\pi \times 10^{2}$
			1.000×10^{9}	N/A	1.000×10^{2}	$2\pi \times 10^{3}$

$$
\begin{aligned}
&+ \beta(1-2\gamma)\sum_{p=1}^{P}\frac{g_{p,k}}{A_{p,k}}\Bigg] S_k\Phi^n \\
&+ \left[(\gamma-1)\varepsilon_0\varepsilon_{\infty,k}+\left(\frac{1}{2}+\beta-\gamma\right)\Delta t\sigma_k\right. \\
&- \beta(1-\gamma)\sum_{p=1}^{P}\frac{g_{p,k}}{A_{p,k}}\Bigg] S_k\Phi^{n-1} \\
&+ \sum_{p=1}^{P}\left(\frac{1}{2}+\beta-\gamma+\frac{\beta B_{p,k}}{A_{p,k}}\right)G_p^n \\
&+ \sum_{p=1}^{P}\left(\frac{1}{2}+\beta-\gamma-\frac{\beta C_{p,k}}{A_{p,k}}\right)G_p^{n-1} = h\Delta t^2. \qquad (31)
\end{aligned}
$$

The same time-stepping procedure used for Debye materials works for Lorentz materials in conjunction with (29) and (31).

F. Numerical Stability

Time-stepping schemes can become unstable. The one we use for Debye materials is unconditionally stable and is considered to be a good option when coping with oscillation errors [14]. This scheme results from the application of Galerkin's method to linear elements in time. However, the same method applied to quadratic elements in time yields a conditionally stable scheme for Lorentz materials. While such a scheme may still be useful in many bioelectric problems, we utilize the general form of time-stepping given by (18) to derive our algorithms for Lorentz materials [14]. The obtained schemes are unconditionally stable for $2\beta \geq \gamma \geq 1/2$ [14].

IV. IMPLEMENTATION

We implement the above algorithms in a MATLAB [16] code. The model geometry and the finite-element mesh are generated with the software package FEMLAB [17] and then exported into the workspace of MATLAB. The solution is displayed either directly in MATLAB or imported in FEMLAB to use other advanced visualization tools.

Consider the computer storage requirements of the algorithms presented in this paper. To calculate the updated global set of nodal potentials Φ^{n+1} for the Debye case, we need to store Φ^n at each node. Further, we must store for each Debye pole p the corresponding $G_{p,k}^n$ in (26) at the nodes of each element. For $G_{p,k}^n$, this means that storage must be provided for each node as many times as the number of elements to which the node belongs.

To calculate the updated global set of nodal potentials Φ^{n+1} for the Lorentz case, we need to store Φ^n and Φ^{n-1} at each node. Further, we must store for each Lorentz pole-pair p the corresponding $G_{p,k}^n$ and $G_{p,k}^{n-1}$ in (29) at the nodes of each element. For $G_{p,k}^n$ and $G_{p,k}^{n-1}$, this means that storage must be provided for each node as many times as the number of elements to which the node belongs.

V. VALIDATION

We now discuss the validation of our theory and numerical algorithm. Our focus is the calculation of the time-varying potential distribution within a dielectric cube. The cube is held at zero potential on one of its faces, and is excited at its opposite face by a normally directed uniform current density having the Gaussian time dependence

$$J_n(m) = \exp\left(-\frac{(m-255)^2}{5469}\right) \qquad (32)$$

where m is the time-step number. At all other cube faces, we assume zero normal current and hence zero normal derivatives of the potential.

The FETD model of this cube consists of 24 linear tetrahedral elements with 14 nodes. We use a time-step of 9.785 ns for the Debye material and 7.828 μs for the Lorentz material. Therefore, in conjunction with the current waveform specified in (32), the excitation spectrum has significant power from dc to several hundred kilohertz for the Debye material, and from dc to several hundred Hertz for the Lorentz material. A total of 512 time-steps $(m = 0, 1, 2, \ldots, 511)$ implements an FETD simulation that is centered in time about the peak of the current excitation. Two cases of dispersive dielectrics are considered. In the first case we simulate the five-pole Debye material reported in [6]. This example is of interest for two reasons: 1) It has a large number of poles, allowing a thorough test of the dispersive algorithm. 2) It provides an excellent approximation of reported experimental data for muscle from 10 Hz to 100 GHz [6]. In the second case we simulate a fictitious Lorentz material having three pole-pairs. This also provides a rigorous test of the dispersive algorithm. Table I provides the Debye and Lorentz

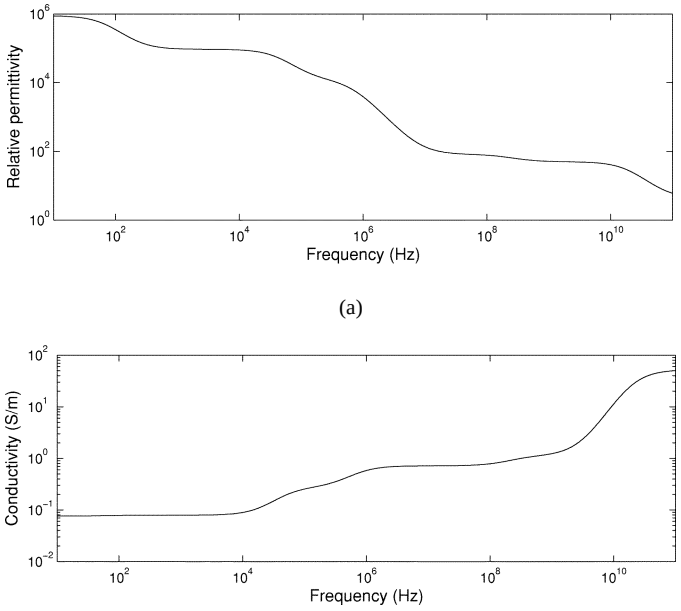

Fig. 1. Frequency-dependent dielectric properties of the five-pole Debye material specified in [6] and Table I: (a) Relative permittivity $\varepsilon_r'(\omega)$. (b) Conductivity $\sigma(\omega) = \sigma_{\rm dc} + \omega\varepsilon_r''(\omega)$.

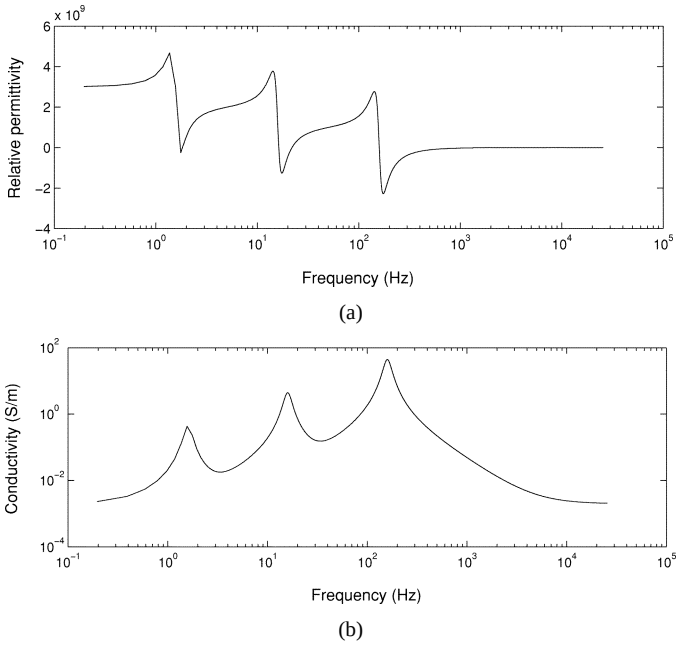

Fig. 2. Frequency-dependent dielectric properties of the three-pole-pair Lorentz material specified in Table I: (a) Relative permittivity $\varepsilon_r'(\omega)$. (b) Conductivity $\sigma(\omega) = \sigma_{\rm dc} + \omega\varepsilon_r''(\omega)$.

parameters for these cases, and Figs. 1 and 2 graph the corresponding material relative permittivity $\varepsilon_r'(\omega)$ and conductivity $\sigma(\omega) = \sigma_{\rm dc} + \omega\varepsilon_r''(\omega)$.

To establish a comparative benchmark, we use the fast Fourier transform (FFT) technique described in [8] to calculate the time-waveform of the electric potential at the excited cube face. The primary computational consideration here is that significant padding of the exciting waveform of (32) is required both before and after the current pulse in order to properly simulate excitation by a single, isolated pulse rather than the

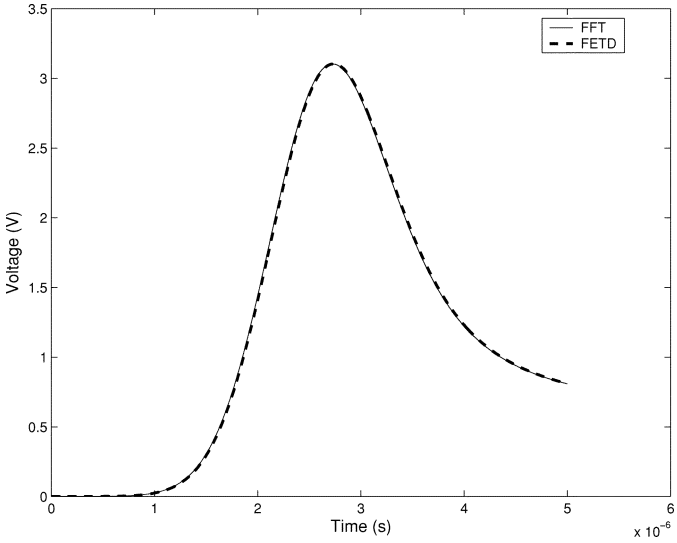

Fig. 3. Agreement of the FETD and benchmark FFT results for the time-waveforms of the calculated potential at the excited cube face for the five-pole Debye material of Fig. 1.

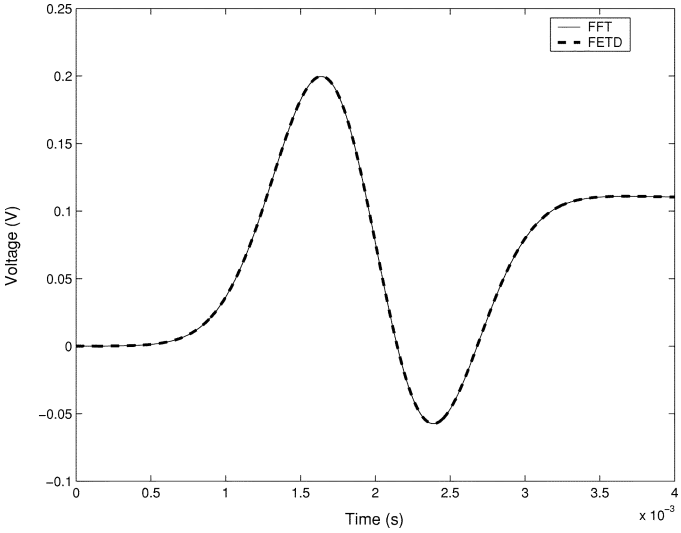

Fig. 4. Agreement of the FETD and benchmark FFT results for the time-waveforms of the calculated potential at the excited cube face for the three-pole-pair Lorentz material of Fig. 2.

periodic pulses implied by the FFT. In fact, we implement this padding by using a total of 262 144 time-steps (each 9.785 ns for the Debye material and 7.828 μs for the Lorentz material) centered about the peak of the current excitation. Figs. 3 and 4 compare the FETD and benchmark FFT results for the time-waveforms of the calculated potential at the excited cube face for the Debye and Lorentz materials of Fig. 1 and Fig. 2, respectively. At all time points, there is a very high level of agreement of about 1% relative to the maximum voltage variation. In fact, the agreement for the Lorentz material case ($\sim$0.07%) is even better than for the Debye case because second-order accurate time-stepping is employed.

VI. Conclusion

This paper reported new FETD algorithms based upon a simple scalar-potential formulation to calculate the time

evolution of the electric potential distribution in materials exhibiting Debye and Lorentz dielectric dispersions. The new algorithms are applicable to the case where eddy currents and wave phenomena are negligible. In general, this case arises for biological tissues of centimeter-to-meter scale exposed to electromagnetic fields having spectra below 1 MHz. These algorithms are based upon the auxiliary differential-equation (ADE) technique previously reported in the context of the FDTD method [11]. For Debye dispersions, we use the unconditionally stable Galerkin time-stepping scheme [14], [15]. For Lorentz dispersions, we use a more general formulation [14] which yields both conditionally and unconditionally stable time-stepping schemes depending upon the choice of parameters. Validation examples for the new FETD algorithms have been provided for generic geometries of tissues having multipole Debye and Lorentz dispersions, which are excited with spectral bandwidths covering the entire range of applicability of the algorithms. We note the following limitations arising from the new FETD algorithms for modeling dispersive materials. First, eddy currents and wave phenomena cannot be modeled. Second, the required computer storage increases linearly with the number of Debye poles or Lorentz pole-pairs being modeled. Third, Cole-Cole dispersions [1], [4] cannot be directly modeled. However, because Cole-Cole dispersions can be accurately approximated with multiple-pole Debye expansions [6], [18], this limitation is not serious. In fact, Fig. 1 and Fig. 3 show validation results for one such approximation. An interesting possibility for future work in this area is the development of FETD algorithms to model nonlinear dispersive biological materials at low frequencies, as encountered in electroporation [19]–[21]. This should be possible based upon the experience of the FDTD community in developing ADE algorithms for nonlinear dispersive materials at optical frequencies [11].

REFERENCES

[1] K. R. Foster and H. P. Schwan, "Dielectric properties of tissues and biological materials: a critical review," *Crit. Rev. Biomed. Eng.*, vol. 17, pp. 25–104, 1989.

[2] C. Gabriel, S. Gabriel, and E. Corthout, "The dielectric properties of biological tissues: I. Literature survey," *Phys. Med. Biol.*, vol. 41, pp. 2231–2249, 1996.

[3] S. Gabriel, R. W. Lau, and C. Gabriel, "The dielectric properties of biological tissues: II. Measurements in the frequency range 10 Hz to 20 GHz," *Phys. Med. Biol.*, vol. 41, pp. 2251–2269, 1996.

[4] ——, "The dielectric properties of biological tissues: III. Parametric models for the dielectric spectrum of tissues," *Phys. Med. Biol.*, vol. 41, pp. 2271–2293, 1996.

[5] L. A. Geddes and L. E. Baker, "The specific resistance of biological material-a compendium of data for the biomedical engineer and physiologist," *Med. Biol. Eng.*, vol. 5, pp. 271–293, 1967.

[6] W. D. Hurt, "Multiterm Debye dispersion relations for permittivity of muscle," *IEEE Trans. Biomed. Eng.*, vol. BME-32, pp. 60–63, 1985.

[7] W. Kuang and S. O. Nelson, "Low-frequency dielectric properties of biological tissues: a review with some new insights," *Trans. ASAE*, vol. 41, pp. 173–184, 1998.

[8] N. S. Stoykov, M. M. Lowery, A. Taflove, and T. A. Kuiken, "Frequency- and time-domain FEM models of EMG: capacitive effects and aspects of dispersion," *IEEE Trans. Biomed. Eng.*, vol. 49, pp. 763–772, Aug. 2002.

[9] R. Plonsey and D. B. Heppner, "Considerations of quasistationarity in electrophysiological systems," *Bull. Math. Biophys.*, vol. 29, pp. 657–664, 1967.

[10] *EMAS User's Manual-Version 4*, J. R. Brauer and B. S. Brown, Eds., Ansoft Corp., Pittsburgh, PA, July 1997.

[11] A. Taflove and S. C. Hagness, *Computational Electrodynamics: The Finite-Difference Time-Domain Method*, 2nd ed. Norwood, MA: Artech House, 2000, pp. 373–410.

[12] J. Jin, *The Finite Element Method in Electromagnetics*, 2nd ed. New York: Wiley, 2002, pp. 549–552.

[13] T. A. Kuiken, N. S. Stoykov, M. Popovic, M. M. Lowery, and A. Taflove, "Finite element modeling of electromagnetic signal propagation in a phantom arm," *IEEE Trans. Neural Systems Rehab. Eng.*, vol. 9, pp. 346–354, Dec. 2001.

[14] O. C. Zienkiewicz and W. L. Wood, "Transient response analysis," in *Finite Element Handbook*, H. Kardestuncer, Ed. New York: McGraw Hill, Inc., 1987, pp. 2.275–2.311.

[15] P. P. Silvester and R. L. Ferrari, *Finite Elements for Electrical Engineers*, 2nd ed. Cambridge, U.K.: Cambridge Univ. Press, 1990, pp. 265–281.

[16] (2002, Oct. 22). *www.mathworks.com* [Online]

[17] (2002, Oct. 22). *www.femlab.com* [Online]

[18] E. S. A. M. Lepelaars, "Electromagnetic pulse distortion in living tissue," *Med. Biol. Eng. Comput.*, vol. 34, pp. 213–220, 1996.

[19] L. Heller and D. Coppola, "Electrically mediated delivery of vector plasmid DNA elicits an antitumor effect," *Gene Therapy*, vol. 9, pp. 1321–1325, 2002.

[20] C.-R. Lin, L.-C. Yang, T.-H. Lee, C.-T. Lee, H.-T. Huang, W.-Z. Sun, and J.-T. Cheng, "Electroporation-mediated pain-killer gene therapy for mononeuropathic rats," *Gene Therapy*, vol. 9, pp. 1247–1253, 2002.

[21] K. N. Kishimoto, Y. Watanabe, H. Nakamura, and S. Kokubun, "Ectopic bone formation by electroporatic transfer of bone morphogenetic protein-4 gene," *Bone*, vol. 31, pp. 340–347, 2002.

Nikolay S. Stoykov (M'00) received the M.S. and Ph.D. degrees in biomedical engineering from the Technical University Ilmenau, Ilmenau, Germany, in 1990 and 1998, respectively.

He is a Research Assistant Professor with the Department of Research, Rehabilitation Institute of Chicago, and with the Department of Physical Medicine and Rehabilitation, Northwestern University, Chicago. His research interests have focused on numerical modeling of bioelectric phenomena.

Todd A. Kuiken (M'99) received the Ph.D. degree in biomedical engineering and the M.D. degree from Northwestern University, Evanston, IL, in 1989 and 1990, respectively.

He was trained in physical medicine and rehabilitation at the Rehabilitation Institute of Chicago, Chicago, IL. He is currently Chief-of-Staff and the Director of Amputee Services at the Rehabilitation Institute of Chicago. He is an Assistant Professor in the Department of PM&R and the Electrical and Computer Engineering Department of Northwestern University. His research interests include the care of amputees, the control of artificial limbs, and myoelectric signal analysis.

Dr. Kuiken is a board certified Physiatrist.

Madeleine M. Lowery (M'00) received the B.E. and Ph.D. degrees from the Department of Electronic and Electrical Engineering, University College Dublin, National University of Ireland, Dublin, Ireland, in 1996 and 2000, respectively.

She is a Research Assistant Professor with the Department of Physical Medicine and Rehabilitation, Northwestern University, Evanston, IL, and the Rehabilitation Institute of Chicago, Chicago, IL. Her research interests include mathematical modeling and analysis of bioelectric signals.

Allen Taflove (M'75–SM'84–F'90) was born in Chicago, IL on June 14, 1949. He received the B.S., M.S., and Ph.D. degrees in electrical engineering from Northwestern University, Evanston, IL in 1971, 1972, and 1975, respectively.

After nine years as a Research Engineer at the IIT Research Institute, Chicago, IL, he returned to Northwestern in 1984. Since 1988, he has been a Professor in the Department of Electrical and Computer Engineering of the McCormick School of Engineering. Currently, he is a Charles Deering McCormick Professor of Teaching Excellence and Master of the Lindgren Residential College of Science and Engineering. Since 1972, he has pioneered basic theoretical approaches and engineering applications of finite-difference time-domain (FDTD) computational electromagnetics. He coined the FDTD acronym in a 1980 IEEE paper, and in 1990 was the first person to be named a Fellow of IEEE in the FDTD area. He authored *Computational Electrodynamics—The Finite-Difference Time-Domain Method* (Norwood, MA: Artech House, In 1995). This book is now in its second edition, coauthored with Prof. Susan Hagness of the University of Wisconsin–Madison. He was the editor of the research monograph, *Advances in Computational Electrodynamics—The Finite-Difference Time-Domain Method* (Norwood, MA: Artech House, In 1998). In addition to the above books, he has authored or coauthored 12 invited book chapters, 73 journal papers, approximately 200 conference papers and abstracts, and 13 U.S. patents. He has been the thesis adviser of 14 Ph.D. degree recipients who hold professorial, research, or engineering positions at major institutions including the University of Wisconsin–Madison, the University of Colorado–Boulder, McGill University, Lincoln Lab, the Jet Propulsion Lab, and the U.S. Air Force Research Lab. Currently, he is conducting research in a wide range of computational electromagnetics modeling problems including the propagation of bioelectric signals within the human body, laser-beam propagation within samples of human blood, UHF diffraction by buildings in urban wireless microcells, microwave cavity resonances in subatomic particle accelerators, electrodynamics of micron-scale optical devices, novel wireless interconnects for ultrahigh-speed digital data buses, and ELF geophysical phenomena.